



Article

# MEX 3D Printed HDPE/TiO<sub>2</sub> Nanocomposites Physical and Mechanical Properties Investigation

Nectarios Vidakis <sup>1,\*</sup>, Markos Petousis <sup>1,\*</sup> , Athena Maniadi <sup>2</sup> , Vassilis Papadakis <sup>3</sup>  and Alexandra Manousaki <sup>4</sup>

<sup>1</sup> Mechanical Engineering Department, Hellenic Mediterranean University, Estavromenos, 71410 Heraklion, Greece; vidakis@hmu.gr

<sup>2</sup> Department of Materials Science and Technology, University of Crete, 70013 Heraklion, Greece; maniadi@materials.uoc.gr

<sup>3</sup> Institute of Molecular Biology and Biotechnology, Foundation for Research and Technology–Hellas, P.O. Box 1527, 71110 Heraklion, Greece; vassilis\_papadakis@imbb.forth.gr

<sup>4</sup> Institute of Electronic Structure and Laser of the Foundation for Research and Technology, Hellas (IESL-FORTH), 71110 Heraklion, Greece; manousa@iesl.forth.gr

\* Correspondence: markospetousis@hmu.gr; Tel.: +30-2810-37-9227

**Abstract:** Aiming to develop more robust, mechanically advanced, Fused Filament Fabrication (FFF) materials, High-Density Polyethylene (HDPE) nanocomposites were developed in the current research work. Titanium Dioxide (TiO<sub>2</sub>) was selected as filler to be incorporated into the HDPE matrix in concentration steps of 0.5, 2.5, 5, and 10 wt.%. 3D printing nanocomposite filaments were extruded in ~1.75 mm diameter and used to 3D print and test tensile and flexion specimens according to international standards. Reported results indicate that the filler contributes to increasing the mechanical strength of the virgin HDPE at certain filler and filler type concentrations; with the highest values reported to be 37.8% higher in tensile strength with HDPE/TiO<sub>2</sub> 10 wt.%. Morphological and thermal characterization was performed utilizing Scanning Electron Microscopy (SEM), Raman, Thermogravimetric Analysis (TGA), and Differential Scanning Calorimetry (DSC), while the results were correlated with the available literature.

**Keywords:** Fused Filament Fabrication (FFF); 3D printing; nanocomposites; flexural strength; tensile strength; High-Density Polyethylene (HDPE); Titanium Dioxide (TiO<sub>2</sub>)



**Citation:** Vidakis, N.; Petousis, M.; Maniadi, A.; Papadakis, V.; Manousaki, A. MEX 3D Printed HDPE/TiO<sub>2</sub> Nanocomposites Physical and Mechanical Properties Investigation. *J. Compos. Sci.* **2022**, *6*, 209. <https://doi.org/10.3390/jcs6070209>

Academic Editor: Francesco Tornabene

Received: 7 June 2022

Accepted: 14 July 2022

Published: 15 July 2022

**Publisher's Note:** MDPI stays neutral with regard to jurisdictional claims in published maps and institutional affiliations.



**Copyright:** © 2022 by the authors. Licensee MDPI, Basel, Switzerland. This article is an open access article distributed under the terms and conditions of the Creative Commons Attribution (CC BY) license (<https://creativecommons.org/licenses/by/4.0/>).

## 1. Introduction

In recent years, a technology gaining momentum and constantly being developed is Additive Manufacturing (AM). AM, and more specifically 3D printing or Fused Filament Fabrication (FFF), which belong to AM technologies, is a fast and cheap parts fabrication method that benefits many industrial sectors, [1] for example, aerospace industries with lightweight components [2]; the biomedical sector, by giving the option of 3D printing of human tissues and implants [2]; and the automotive industry by helping to produce rapid prototypes for fast and feasible evaluation before mass part production [3].

FFF or Material Extrusion 3D printing (MEX3DP), includes a vast agenda of applicable materials. The literature reports developments in sustainable additive manufacturing by studying the mechanical and thermal behavior of Acrylonitrile Butadiene Styrene (ABS) in FFF and after repeated heating cycles and extruded material reprocessing [4,5]. The literature also reports similar studies with Polypropylene (PP) [6], and Polyethylene (PE) (with the brand name Kritilen, procured from its manufacturer Plastika Kritis S.A., Heraklion, Greece) [7]. Moreover, studies on FFF and the mechanical properties of 3D printed parts report that 3D printing parameters can directly affect the mechanical properties of the final part [8–13]. Furthermore, regarding common materials used in FFF, such as ABS, and Polylactic Acid (PLA), studies have shown that adding nano or micro fillers into a polymer matrix can successfully enhance the mechanical properties of the unfilled matrix [14–18].

One newly added material to this method is High-Density Polyethylene (HDPE). HDPE is a thermoplastic material, a commodity polymer found in every household nowadays, and is used to produce a vast number of items and parts. The polyethylene group of polymers embraces some of the most applicable polymers nowadays due to their flexibility of applications. LDPE, HDPE, and PP are the most popular thermoplastics, with uses including containers, pipes, toys, and bags (LDPE), gas pipes (HDPE) [19], industrial wrappings, housewares, and film [19–22] and electrical components and automotive parts (PP) [22,23]. HDPE plastic is used in a variety of industries to replace heavy parts with lighter ones that can withstand equivalent loads while delivering rigid strength, corrosion resistance, and environmental friendliness. Because of its great recyclability and cost-effectiveness, HDPE is also recognized as a material that is suited for ecologically responsible and cost-effective production [19].

HDPE is currently being researched for 3D printing, and it is being further developed with the addition of nano/micro fillers to enhance the mechanical and/or electrical properties of the unfilled HDPE matrix. Literature includes HDPE with the addition of carbon nanotubes [24], fly ash cenospheres [25–27], glass micro balloons [28–30], carbon [31], calcium carbonate [32], and graphite nanofibers [33]. Moreover, literature reports that quantity-wise, HDPE with nanofillers in concentrations below 5 wt.% can significantly improve the mechanical strength of the HDPE matrix when used in 3D printing [34–36].

Moreover, research was done in literature on HDPE and its electrical and thermal properties and how they change when nano or micro fillers are added. Literature contains reports with HDPE doped with Titanium Dioxide (TiO<sub>2</sub>) [36–38], Tin Oxide (SnO<sub>2</sub>) [35–39], alumina [40,41], and Zinc Oxide (ZnO) [42]. All the above research was done upon injection molded specimens or machined specimens from bulk materials. Limited research was done on HDPE nanocomposites for rapid tooling applications, but with no available results on the mechanical properties of 3D printed specimens [43].

Regarding HDPE with commercially available fillers such as Titanium Dioxide (TiO<sub>2</sub>), there is limited or no literature available yet reporting results on the mechanical properties of 3D printed specimens. Current research aims to develop and study novel and more robust HDPE nanocomposites comprised of HDPE matrix with the implementation of TiO<sub>2</sub> in specific by-weight concentrations. Moreover, another goal of the study was to produce nanocomposites with enhanced mechanical properties from popular materials in industrial applications. Another scope of this study is to help achieve better printability for HDPE composites and nanocomposites while using commercial 3D printers and extruders. Novel nanocomposite filaments were produced utilizing melt extrusion in this work, with HDPE matrix filled with TiO<sub>2</sub> nanoparticles in certain filler loadings. More specifically, there was a 28.5% increase in tensile strength with HDPE with 10 wt.% filler loading and a 77.6% increase in flexural strength with HDPE with 2.5 wt.% filler. Results of 3D printed specimens showed an increase in both tensile strength and flexural strength with the incorporation of TiO<sub>2</sub> particles. Morphological analysis was also done with Scanning Electron Microscopy (SEM) and Raman spectroscopy, while the thermal properties of the fabricated materials were examined via Thermogravimetric analysis (TGA) and Differential Scanning Calorimetry (DSC). Such results show high potential for use of such nanocomposites in 3D printing applications requiring an enhanced mechanical response from the HDPE material, further exploiting the advances of AM.

## 2. Materials and Methods

### 2.1. Materials

The polymer matrix used in this work in the form of powder was Kritilen High-Density Polyethylene, industrial grade. Regarding the properties of Kritilen pure HDPE, the supplier indicates that the density of the material is 0.960 g/cm<sup>3</sup>, the melt Mass-Flow Rate (MFR) (190 °C/2.16 kg) is 7.5 g/10 min while the Vicat Softening Temperature is 127 °C. Moreover, no plasticizers or additives were utilized. Regarding the nanofiller introduced in this work,

Degussa Evonik P25 (Essen, Germany) with an average particle size of 25–50 nm Titanium dioxide (TiO<sub>2</sub>) was chosen as the nanofiller.

## 2.2. Nanocomposites and Microcomposites Fabrication

The overall workflow and steps followed in this research are depicted below in Figure 1. As the first step, all materials were mixed in certain filler percentages and then were dried at 70 °C for 48 h before extruding. The filler concentrations chosen for this study, are the same used in all the above research scenarios, i.e., 0, 0.5, 2.5, 5, 10, and 20 wt.%.

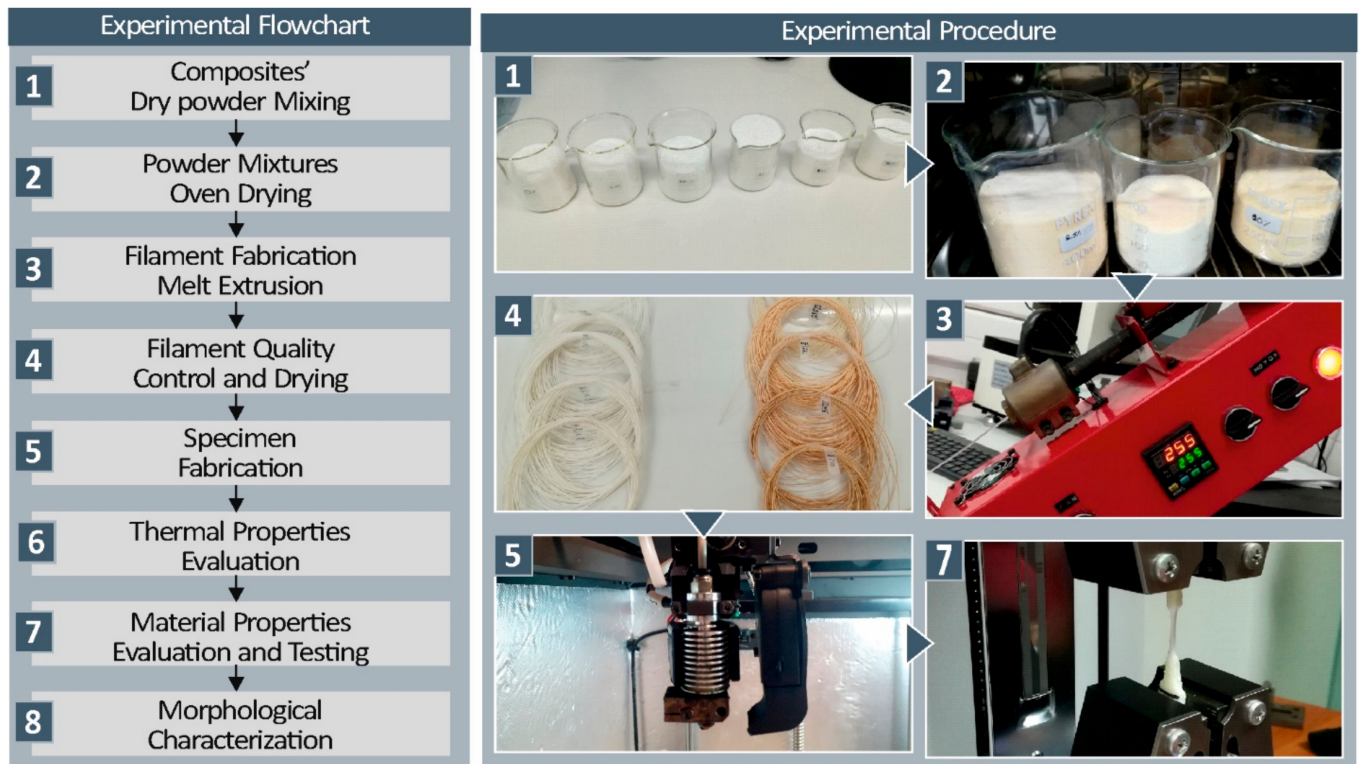


**Figure 1.** Workflow methodology that was followed in this work.

Material extrusion was done via a single screw desktop extruder, Noztek Pro (Shoreham-by-Sea, UK), preheated to 200 °C. Preheat was applied so any humidity left in the extrusion system was eliminated before material extrusion. The extrusion working temperature was found experimentally to be around 255 °C. This temperature was validated using TGA analysis, which did not cause degradation to the material. This working temperature is derived experimentally by seeking the softening/melting point of HDPE while having the necessary working pressure and flow to extrude the proper dimension filament.

HDPE itself has the difficulty of being quite viscous when heated, dissipating heat very slowly, and sticking with ease to surfaces. To overcome difficulties extruding this type of material while maintaining a stable filament diameter, an extruder fan was activated, and two more fans were placed 20 cm away from the extruder nozzle to cool the extruded filament down in a controlled way. The processability of the fabricated filament became more difficult when the filler concentration was above 10 wt.% which created clogs in the extruder nozzle and the 3D printing nozzle, making the 3D printing of the specimens faulty. Thus, the filler maximum concentration for the HDPE matrix was set at 20 wt.%. 3D printing nanocomposites with concentrations higher than 20 wt.% was not possible.

Afterwards, the filament afterward was carefully examined, and measurements were taken to validate the stable filament diameter and to ensure that the filament will be able to pass through the nozzle of the 3D printer without clogging.

### 2.3. Specimens Fabrication

Before the specimens' fabrication, all the fabricated filaments were oven-dried at 70 °C for at least 24 h to remove any humidity that may cause bubbles or faulty 3D printed specimens. The filaments then were used through an Intamsys Funmat HD (Shanghai, China) MEX 3D printer without the use of any 3D printing aids such as glue or tape. The 3D printing temperature was kept constant at 250 °C. The printing temperature was also found experimentally.

For tensile experiments, a total of seven specimens were fabricated, out of which randomly selected five specimens were mechanically tested. All the specimens were fabricated in accordance with ASTM D638 Standard (type V dogbone specimens, with overall width 10 mm, length 65 mm, and 3.2 mm thickness). Regarding the specimens fabricated for the flexural experiments and more specifically, 3-point bending, seven specimens were 3D printed according to ASTM D790 (prismatic specimens with 12.7 mm width, 64 mm length, and 3.2 mm thickness) standard while five randomly selected specimens were mechanically tested in the flexion scenario.

### 2.4. Mechanical Characterization

The mechanical characterization in both tension and flexion cases was performed utilizing an IMADA MX2 (Northbrook, IL, USA) apparatus with standardized grips for each case. The machine's chuck speed parameters were kept constant at a 10 mm/min speed as the international ASTM standards require.

For the micro-hardness measurements, the ASTM E384-17 standard was followed. Proper surface finish of the test specimens was ensured before the evaluation. The method applied in this case for measuring the microhardness was the micro-Vickers method, with a 0.1 kg selected force scale (0.981 N) and 10 s indentation time. A typical Vickers diamond pyramid was used as an indenter (apex angle of 136°), which was forced onto a polished surface of the specimens. The area of the remaining indentation, after the retraction of the diamond pyramid, is calculated directly by the device from the remaining imprint's mean average of the diagonals, visible in the device's microscope. Experiments were performed with the aid of an Innova Test 400-Vickers (Innovatest Europe BV, Maastricht, The Netherlands) apparatus.

### 2.5. Thermal Properties Investigation

Thermogravimetric Analysis (TGA) was used to determine the critical degradation temperature of the HDPE pure material and its nanocomposites used in this study so that the optimum extrusion and 3D printing temperatures could be determined. The measurements were collected using a Perkin Elmer Diamond TG/TDA (Waltham, MA, USA) with a room temperature (32 °C) to 550 °C heating cycle with a 10 °C/min heating step. As a purge gas, nitrogen was used.

The effect of filler concentration on the melting point ( $T_m$ ) and shift in the degree of crystallinity of the samples was further investigated using Differential Scanning Calorimetry (DSC), following the literature [44]. The degree of crystallization was calculated using the following equation:

$$X_c(\% \text{crystallinity}) = \frac{\Delta H_m}{\Delta H_0} * 100\% \quad (1)$$

where:  $\Delta H_m$  is the melting enthalpy (the area under the melting curve), and  $\Delta H_0$  is a theoretical value of the melting enthalpy of 100% crystalline HDPE. The value  $\Delta H_0 = 293 \text{ J/g}$  was used in a degree of crystallinity calculation. The measurements were conducted using a Perkin Elmer Diamond DSC (Waltham, MA, USA) with a temperature cycle of 50 °C to 300 °C with a 10 °C/min heating step and then cooling back down to 50 °C. The heating was done with nitrogen.

## 2.6. Morphological and Structural Characterization

Scanning electron microscopy (SEM) was done with a JEOL JSM 6362LV (Jeol Ltd., Peabody, MA, USA) electron microscope in high-vacuum mode at 20 kV acceleration voltage on sputtered-gold coated specimens. Energy Dispersive X-ray Analysis (EDX) was performed on non-sputtered specimens. The specimens were studied to identify the fracture mode and their layer fusion.

Raman measurements were performed with a modified LabRAM HR Raman Spectrometer (HORIBA Scientific, Kyoto, Japan). Raman excitation was achieved with a 532 nm central wavelength solid-state laser module with a maximum laser output power of 90 mW. The microscope is coupled with a 50× microscopic objective lens with a 0.5 numerical aperture and 10.6 mm working distance (LMPlanFL N, Olympus, Hongkong, China) that delivered the excitation light and collected the Raman signals. A neutral density filter of 50% transmittance was used, which resulted in 20 mW of power on the sample. The laser spot size was approximately 1.7 μm laterally, and about 2 μm axially. A 600 groove grating was used resulting in a Raman spectral resolution of around 2 cm<sup>-1</sup>. The Raman spectral range was set to be from 400 to 3100 cm<sup>-1</sup>, resulting in two optical windows per point. The acquisition time for each measurement was 3 s and with 5 accumulations at each point.

## 3. Results & Discussion

### 3.1. Mechanical Characterization

Figure 2 below presents the overall results data of (a) tensile stress vs. strain graph for HDPE/TiO<sub>2</sub> in all filler concentrations studied, (b) comparative tensile strength graph for each material studied, and (c) tensile mod. of elasticity for all the materials studied.

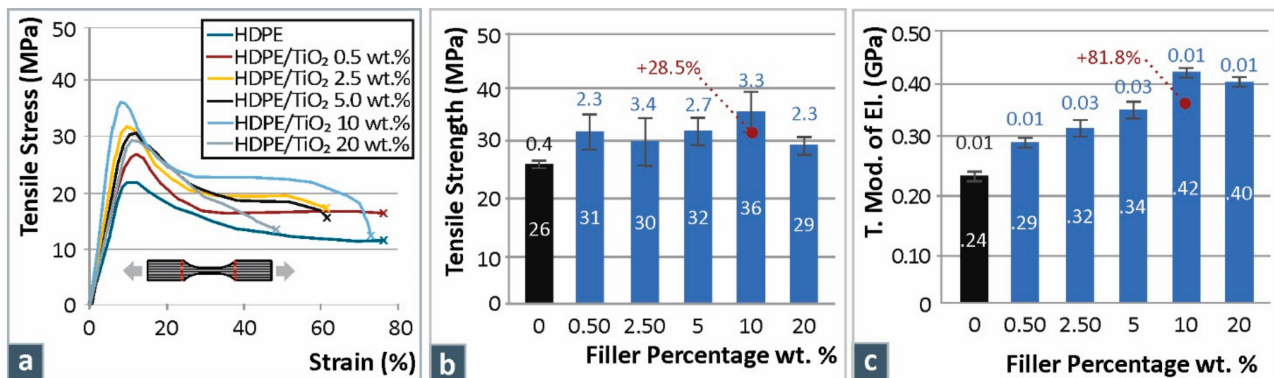


**Figure 2.** Overall (a) tensile stress vs. strain graphs for HDPE/TiO<sub>2</sub>, (b) comparative tensile strength graph, and (c) tensile mod. of elasticity for all the materials studied.

From the resulting data above, it was evident there is an increase in tensile strength of 28.5% in the case of HDPE doped with TiO<sub>2</sub> nanoparticles 10 wt.% when compared to the unfilled polymer matrix. Regarding tensile modulus of elasticity, there is a visible trend that tensile modulus increases with the filler percentage in all cases studied. No literature is yet available on HDPE 3D printed nano/micro composites to correlate these mechanical properties findings. Research is available on HDPE with TiO<sub>2</sub> as filler, but it is with injection-molded specimens [36,37], and in these works, they don't report mechanical properties.

Moreover, from the experimental data and the tensile stress/strain curves in all cases studied, it was apparent that the HDPE materials exhibited a high strain rate and deformation before failing. The specimens filled with TiO<sub>2</sub> showed overall less deformation.

Figure 3 shows the overall (a) flexure stress vs. strain graph for HDPE/TiO<sub>2</sub>, (b) comparative flexure strength graph, and (c) flexural mod. of elasticity for all the materials studied. While Figure 4 presents the overall (a) tensile toughness of HDPE with TiO<sub>2</sub> filler at 0, 0, 5, 10, and 20 wt.%; and (b) flexure toughness of HDPE with TiO<sub>2</sub> filler at 0, 0, 5, 10, and 20 wt.%.

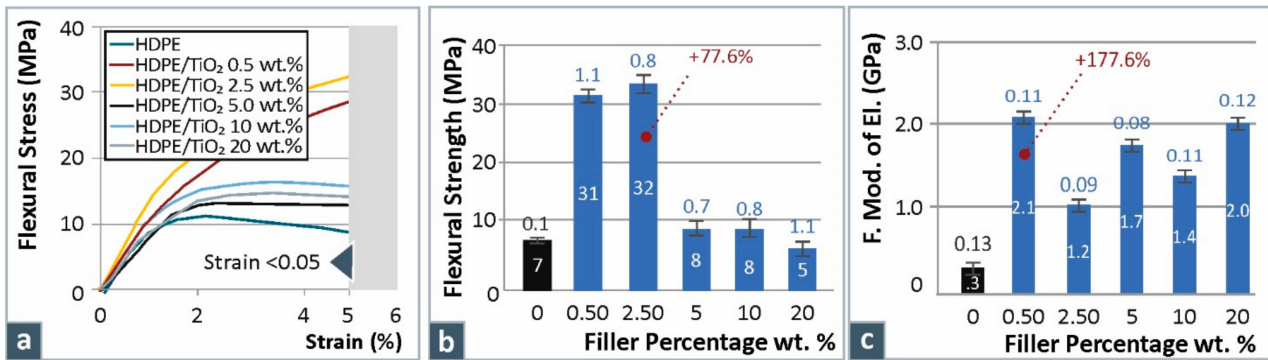


**Figure 3.** Overall (a) flexure stress vs. strain graphs for HDPE/TiO<sub>2</sub>, (b) comparative flexure strength graph, and (c) flexural mod. of elasticity for all the materials studied.

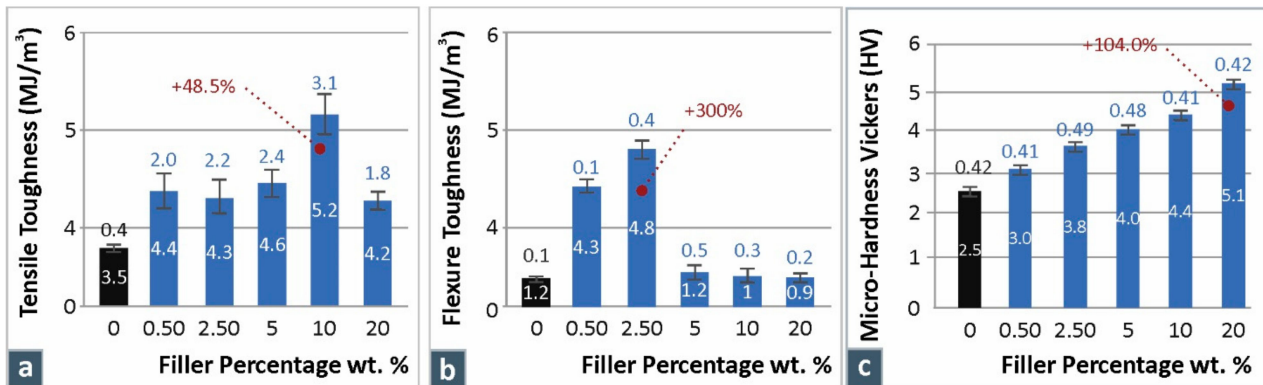


**Figure 4.** Overall (a) tensile toughness of HDPE with TiO<sub>2</sub> filler at 0, 0.5, 2.5, 5, 10, and 20 wt.%; and (b) flexure toughness of HDPE with TiO<sub>2</sub> filler at 0, 0.5, 2.5, 5, 10, and 20 wt.%; (c) the overall micro-hardness Vickers results for HDPE unfilled and HDPE with TiO<sub>2</sub> materials.

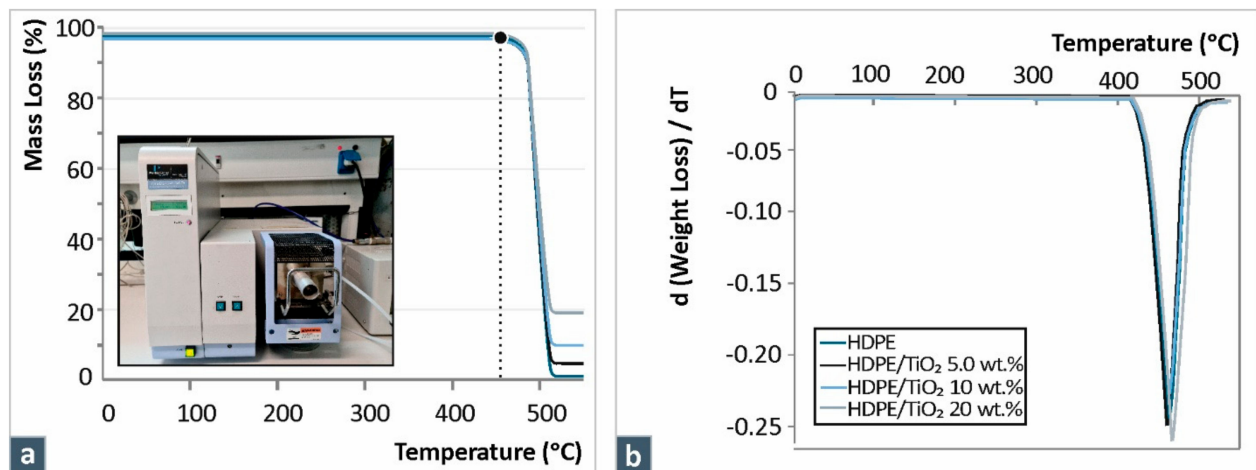
As for the flexural results, data indicated that there is a notable 77.6% increase in flexural strength when comparing HDPE/TiO<sub>2</sub> 2.5 wt.% to unfilled HDPE polymer. The highest flexural modulus of elasticity was at 0.5 wt.% filler concentration when compared to unfilled HDPE. No literature is yet available on HDPE 3D Printed nanocomposites with which to correlate these mechanical findings. Research showed that there are a few publications available, but they are on injection-molded specimens [36,37], and they do not report any findings on mechanical properties with which to correlate the above findings of this work regarding the mechanical response of the nanocomposites. It should be noted that the tensile and the flexural tests do not follow the same trend regarding the mechanical test results as the filler loading increases. In each type of test, different types of loadings are applied and different types of stresses are developed in the materials. Therefore, different mechanical tests are necessary to evaluate the response of the nanocomposites under different loading scenarios, and differences in the materials' responses to the different tests are expected.

Figure 4 presents (a) the comparative graphs for tensile toughness with HDPE unfilled and HDPE with TiO<sub>2</sub> at specific filler loadings, (b) the comparative graphs for flexure toughness with HDPE unfilled and HDPE with TiO<sub>2</sub> at specific filler loadings, and (c) the overall micro-hardness Vickers results for HDPE unfilled and HDPE with TiO<sub>2</sub> materials studied in this work. The toughness results in Figure 4a,b show the same trend as the results in Figures 2b and 3b. Regarding the tensile toughness, results indicate an increase of 48.5% with the introduction of 10 wt.% TiO<sub>2</sub>, while regarding the flexural toughness there is an increase of 300% with the 2.5 wt.% filler loading.

From Figure 4c, it is evident that Vickers microhardness increases with the filler loading, resulting in a 104% increase in microhardness at 20 wt.% filler loading. The literature reports similar values regarding HDPE with nanofillers and microhardness Vickers [45].

### 3.2. Thermal Properties Investigation

Figure 5 below presents the overall (a) TGA data for HDPE with TiO<sub>2</sub> filler at 0, 5, 10, and 20 wt.%; and (b) weight loss rate.



**Figure 5.** (a) TGA data for HDPE with TiO<sub>2</sub> filler at 0, 5, 10, and 20 wt.%; and (b) weight loss rate.

As is shown in Figure 5a, the material's weight loss curves are similar up to the point where the materials start to rapidly degrade. This is an indication that the addition of the TiO<sub>2</sub> fillers in the HDPE matrix material did not affect the thermal stability of the polymer throughout the thermal analysis.

From the above TGA results in Figure 5a,b, it can be validated that the remaining percentage in each case is the corresponding weight percentage of the filler used for the fabrication of the nano/micro composite filaments. In all cases studied, the remaining percentage of the nano/micro filler is slightly less than the percentage used. For example, in the case of HDPE/TiO<sub>2</sub> 20 wt.%, the remaining percentage according to TGA analysis was 18.77%. This minor difference can be attributed to the instrument's accuracy or losses caused by either initial extrusion of the filament or losses from the 3D printing procedure.

From the DSC analysis in Figure 6, it was proven that the use of fillers slightly shifts and increases the melting point ( $T_m$ ) when compared to the unfilled HDPE matrix. This increase is evident with the increase of the filler percentage in all cases of TiO<sub>2</sub>. Regarding the degree of crystallinity calculations, no significant differences were found, with the results being similar between the different materials studied.

### 3.3. Morphological and Structural Characterization

In Figure 7 are presented the SEM images of (a) HDPE unfilled materials' 3D printed specimen fracture area, and (b) HDPE unfilled materials' 3D printed specimen side area. Note that the selected specimens are random tensile specimens in each case.

Moreover, Figure 8 depicts the SEM images of (a) HDPE/TiO<sub>2</sub> 0.5 wt.% materials' 3D printed specimen fracture area, (b) HDPE/TiO<sub>2</sub> 2.5 wt.% materials' 3D printed specimen fracture area; (c) HDPE/TiO<sub>2</sub> 5 wt.% materials' 3D printed specimen fracture area; (d) HDPE/TiO<sub>2</sub> 10 wt.% materials' 3D printed specimen fracture area. Note that the selected specimens are random tensile specimens from each case.

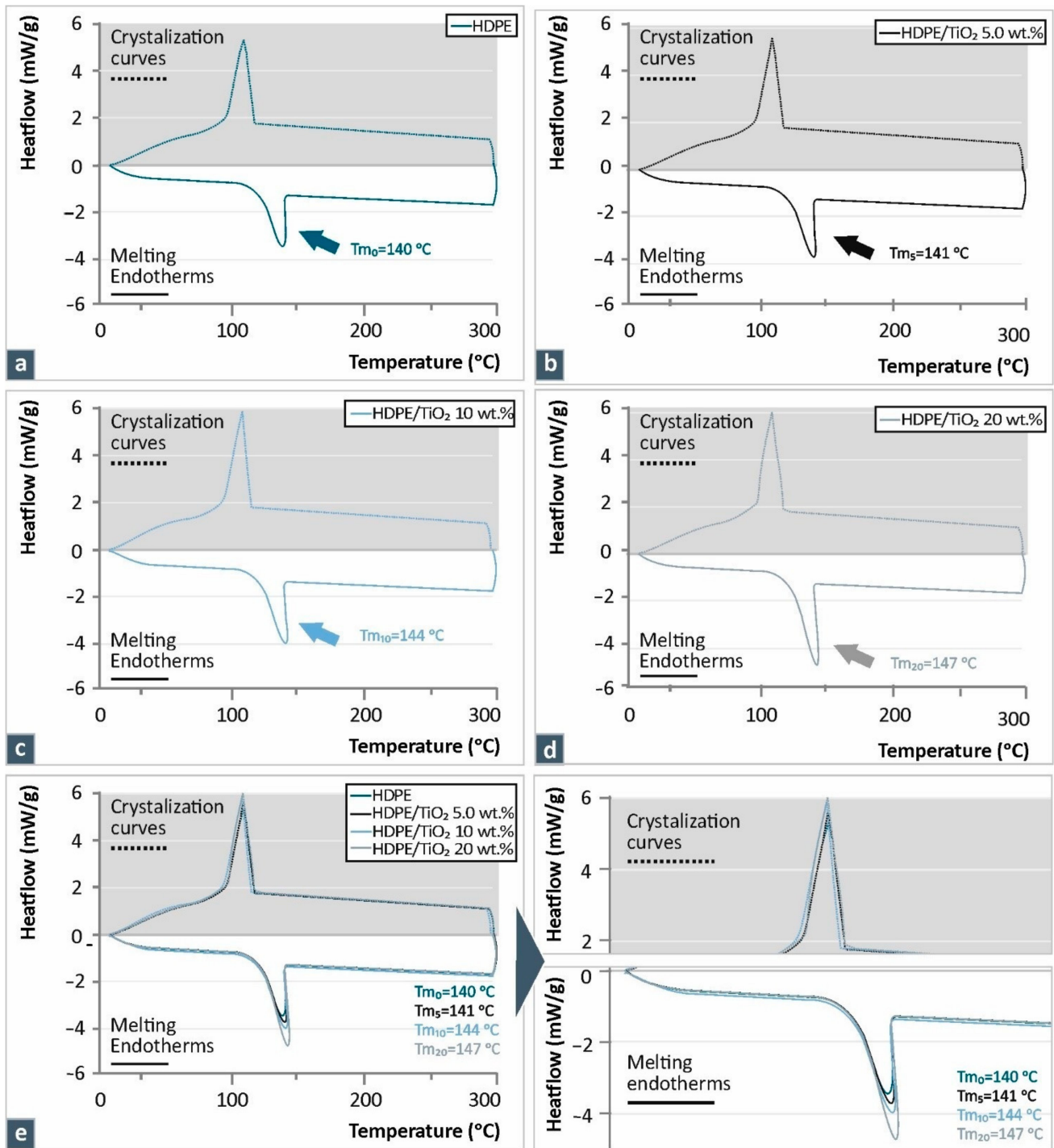


**Figure 6.** Overall DSC data for HDPE with TiO<sub>2</sub> filler at (a) 0, (b) 5, (c) 10, and (d) 20 wt.%; (e) DSC comparative data for HDPE with TiO<sub>2</sub> fillers all concentrations.

Furthermore, in Figure 9 presents the SEM images of (a) HDPE 0.5 wt.% TiO<sub>2</sub> printed specimen side area at 500 μm, (b) HDPE 0.5 wt.% TiO<sub>2</sub> printed specimen side area at 100 μm (c) HDPE 2.5 wt.% TiO<sub>2</sub> printed specimen side area at 500 μm, (d) HDPE 2.5 wt.% TiO<sub>2</sub> printed specimen side area at 10 μm; (e) HDPE 5 wt.% TiO<sub>2</sub> printed specimen side area at 500 μm, (f) HDPE 5 wt.% TiO<sub>2</sub> printed specimen side area at 100 μm, (g) HDPE 10 wt.% TiO<sub>2</sub> printed specimen side area at 500 μm, (h) HDPE 10 wt.% TiO<sub>2</sub> printed specimen side area at 100 μm. Note that the selected specimens are random tensile specimens in each case.

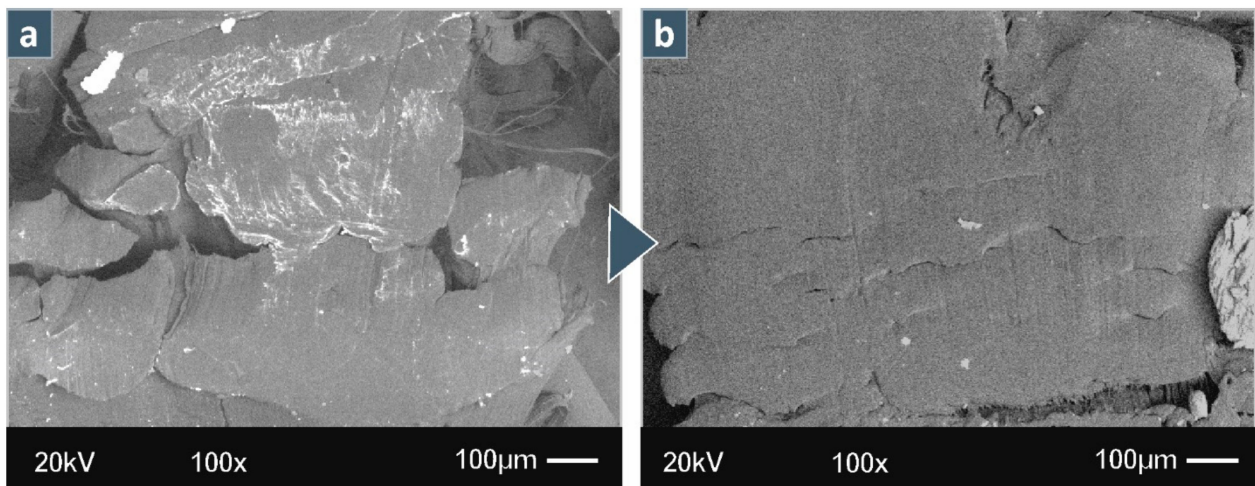


**Figure 7.** SEM images of (a) HDPE unfilled materials' printed specimen fracture area, (b) HDPE unfilled materials' printed specimen side area.

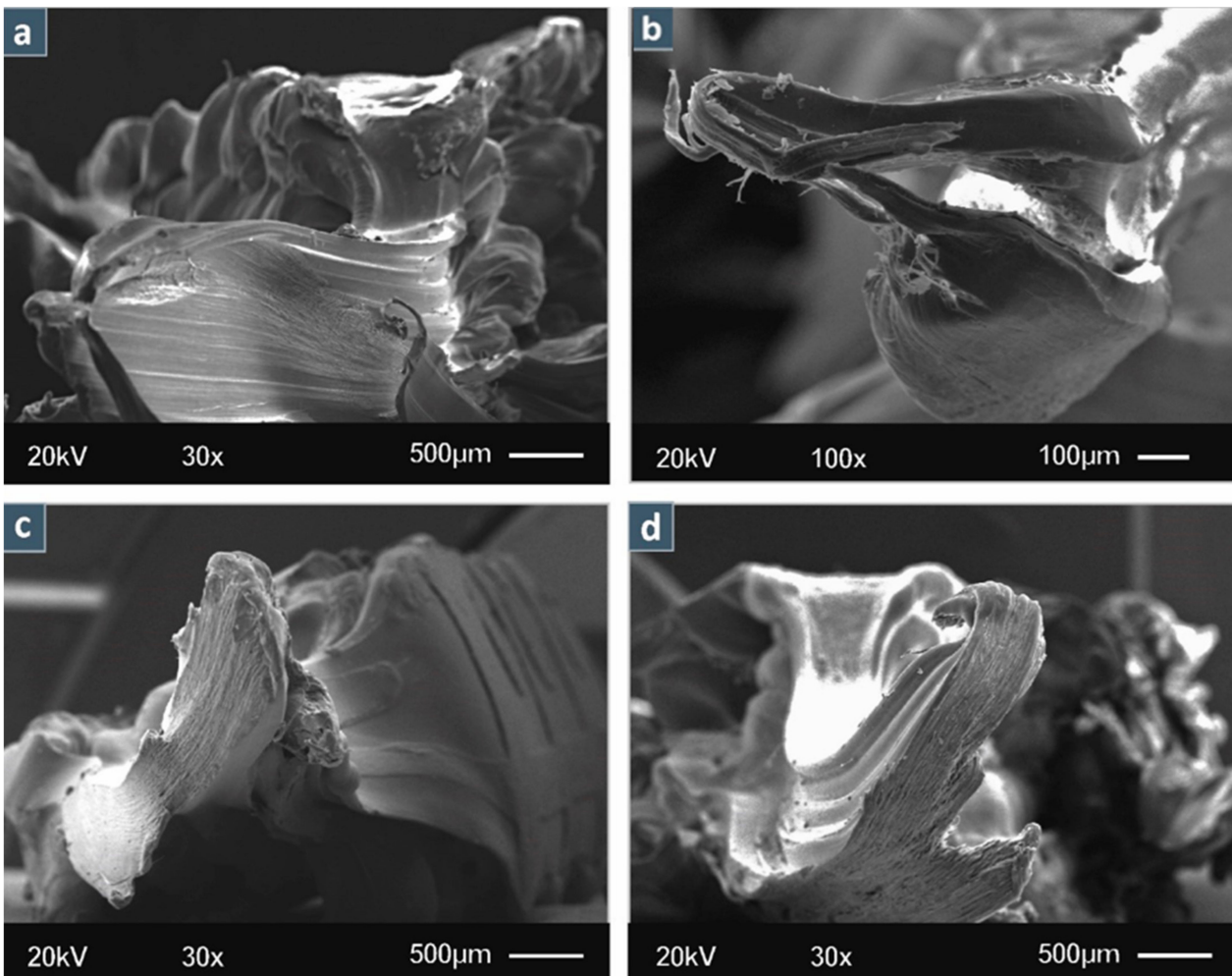


**Figure 8.** SEM images of (a) HDPE/TiO<sub>2</sub> 0.5 wt.% materials' printed specimen fracture area, (b) HDPE/TiO<sub>2</sub> 2.5 wt.% materials' printed specimen fracture area; (c) HDPE/TiO<sub>2</sub> 5 wt.% materials' printed specimen fracture area; (d) HDPE/TiO<sub>2</sub> 10 wt.% materials' printed specimen fracture area. Note that the selected specimens are random tensile specimens in each case.

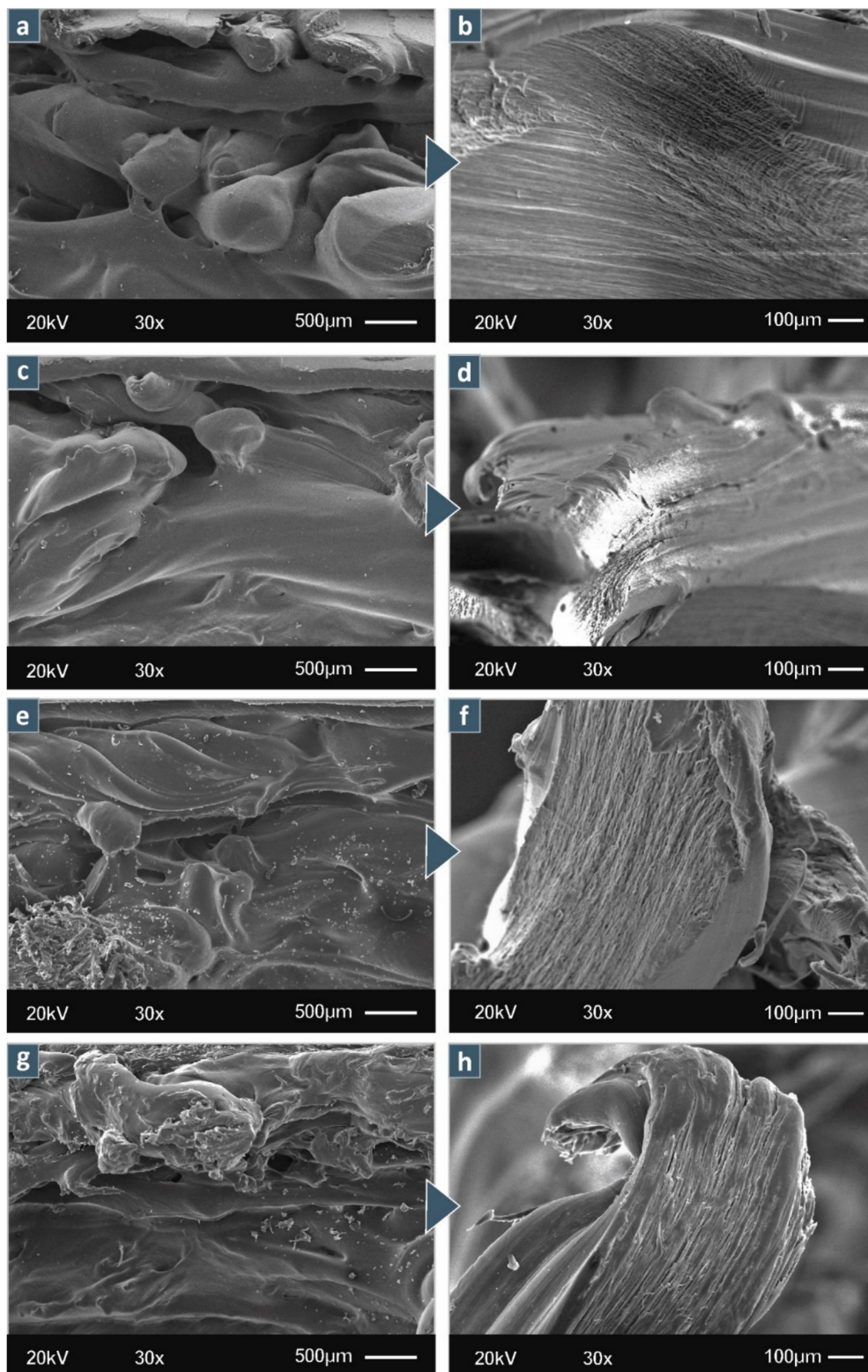


**Figure 9.** SEM images of (a) HDPE 0.5 wt.% TiO<sub>2</sub> printed specimen side area at 500 μm, (b) HDPE 0.5 wt.% TiO<sub>2</sub> printed specimen side area at 100 μm (c) HDPE 2.5 wt.% TiO<sub>2</sub> printed specimen side area at 500 μm, (d) HDPE 2.5 wt.% TiO<sub>2</sub> printed specimen side area at 10 μm; (e) HDPE 5 wt.% TiO<sub>2</sub> printed specimen side area at 500 μm, (f) HDPE 5 wt.% TiO<sub>2</sub> printed specimen side area at 100 μm, (g) HDPE 10 wt.% TiO<sub>2</sub> printed specimen side area at 500 μm, (h) HDPE 10 wt.% TiO<sub>2</sub> printed specimen side area at 100 μm. Note that the selected specimens are random tensile specimens in each case.

In the SEM images captured of the samples, no agglomerations were observed. Additionally, the results of the mechanical tests showed deviation within acceptable limits. These observations provide an indication of a similar and uniform dispersion of the filler in the matrix, otherwise, significant differences would have been recorded.

As the SEM images indicate, for HDPE with TiO<sub>2</sub> there is an evident reduction in ductility in the 3D printed specimens as the filler percentages increase. From Figures 7 and 8, the fracture area begins failing in a less ductile manner as the fracture neck strands slightly disappear as the filler percentage increase. This can be attributed to the fillers occupying free space positions inside the polymer chain, restricting the chain's mobility. Tensile strength results, along with flexural strength results, correlate with the above statement as the chain mobility is linked to the mechanical properties of the final specimens [46].

Regarding the layer fusion of the materials studied, SEM images from the right columns of Figures 7 and 9 indicate a slight change in the layer fusion in 3D printed specimens, specifically in specimens with 5 wt.% and 10 wt.% in which the layer fusion seems to be more uniform, with no visible gaps, as the images of 0.5 and 2.5 wt.% indicate. The other specimens showed no significant changes in layering fusion and 3D printing deposition when compared to unfilled HDPE polymer. A possible reason why the layer deposition slightly differs in the specimens of 5 and 10 wt.% filler could be that the filament's diameter shifts due to the material's high shrinkage rate upon cooling.

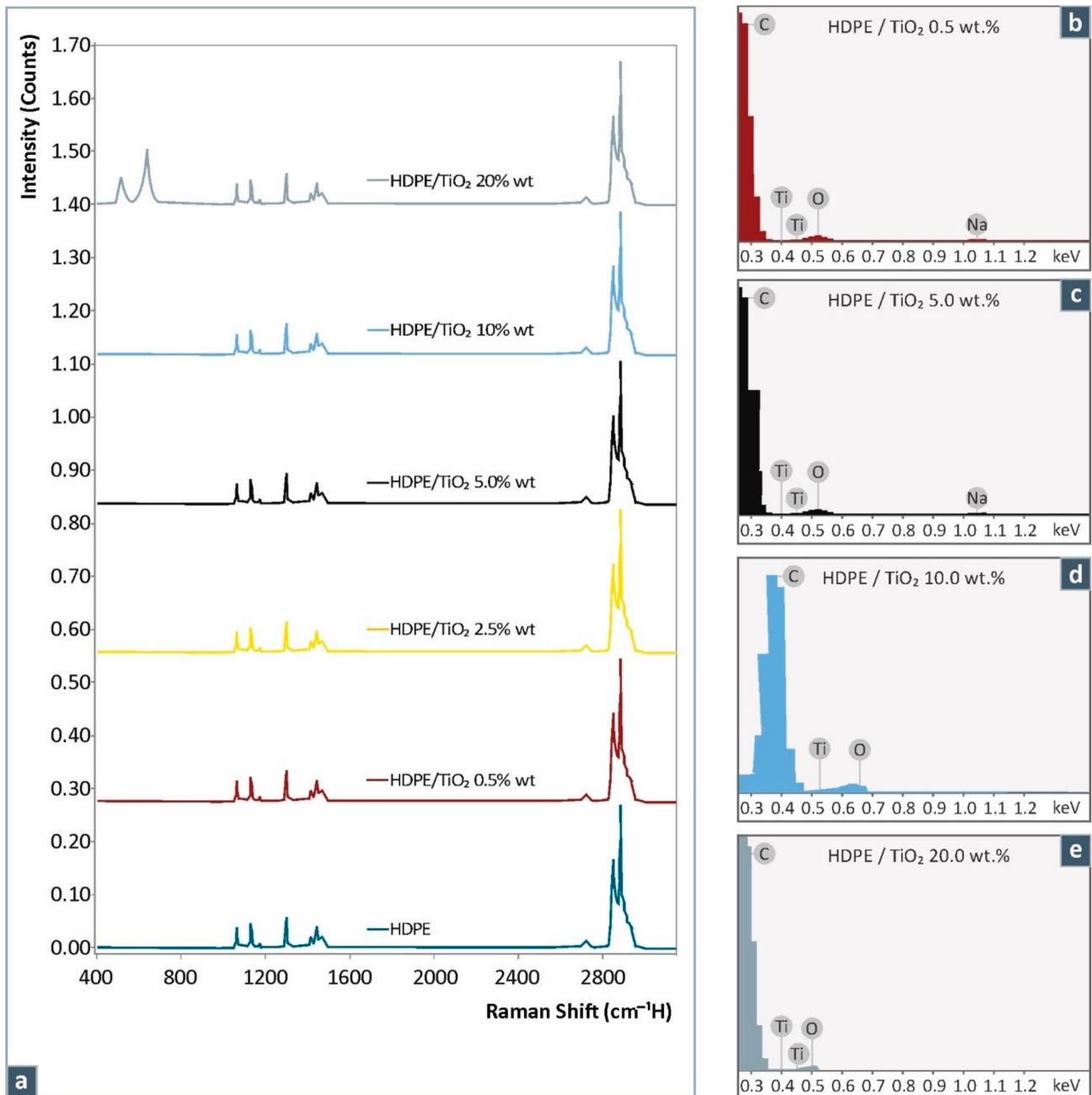
The overall printability of the specimens was found to be more difficult over 10% filler loadings, as the 3D printer nozzle tended to clog and burn the filament. Shrinkage, layer deposition, and fusion did not seem to be affected significantly by the filler concentration increase as the SEM analysis suggests. Thermal analysis of the 3D printed specimens also showed no shift in T<sub>g</sub> temperature of the materials studied herein, thus there was no significant alteration in the polymer's chain mobility.

Figure 10 below presents, (a) Raman Spectra for HDPE materials with TiO<sub>2</sub> filler and EDS results for filler concentrations (b) 0.5, (c) 5, (d) 10, and (e) 20 wt.%. From the EDS compositional analysis, the major elements of HDPE and TiO<sub>2</sub> were identified without any residues from other materials or dirt present.

As is seen in Figure 10 the major Raman peaks are from HDPE Pure. C-O-C stretching was found at 1064, 1131, and 1297 cm<sup>-1</sup>. CH<sub>3</sub> deformation and CH<sub>2</sub> deformation were found at 1418 and 1441 cm<sup>-1</sup> respectively. Lastly, CH<sub>2</sub> symmetric stretching was identified at 2850 cm<sup>-1</sup> and C-H antisymmetric stretching at 2883 cm<sup>-1</sup>. All samples that had TiO<sub>2</sub> mixed, presented the related Raman peaks at 515 cm<sup>-1</sup> and 638 cm<sup>-1</sup> related to the TiO<sub>2</sub> anatase crystal phase [47]. As expected, the intensity of those Raman peaks increases together with the concentration of TiO<sub>2</sub> in the HDPE samples. Please see Table 1.

**Table 1.** Major Raman peaks identified and their related assignments.

Wavenumber (cm <sup>-1</sup> )	Raman Peak Assignment
515	Anatase crystal phase of TiO <sub>2</sub> [47]
638	Anatase crystal phase of TiO <sub>2</sub> [47]
1064	C-O-C stretching [48]
1131	C-O-C stretching [49]
1297	C-O-C stretching [48]
1418	CH <sub>3</sub> deformation [48]
1441	CH <sub>2</sub> deformation [48,50]
2850	CH <sub>2</sub> symmetric stretching [51]
2884	C-H antisymmetric stretching [52]



**Figure 10.** (a) Raman Spectra for HDPE with TiO<sub>2</sub> filler and EDS results for filler concentrations (b) 0.5, (c) 5, (d) 10, and (e) 20 wt.%.

#### 4. Conclusions

In the current research and for the first time in the literature, HDPE nano and micro composites were prepared for MEX 3D printing by implementing TiO<sub>2</sub> fillers at various wt.% concentrations in an HDPE polymer matrix to investigate the effect on the mechanical properties of the polymer matrix. The thermal properties and morphological characteristics of the 3D printed specimens were also studied with TGA, DSC, and SEM analyses.

The overall results of this study (Figure 11) showed that through the implementation of TiO<sub>2</sub> particles in specific filler loadings, the overall mechanical strength of the HDPE polymer matrix can be significantly increased. It was found that there is an increase of 28.5% in tensile strength derived from HDPE with 10 wt.% filler loading, while there is an increase of 81.8% in flexural strength with the introduction of 10 wt.% to HDPE polymer matrix.

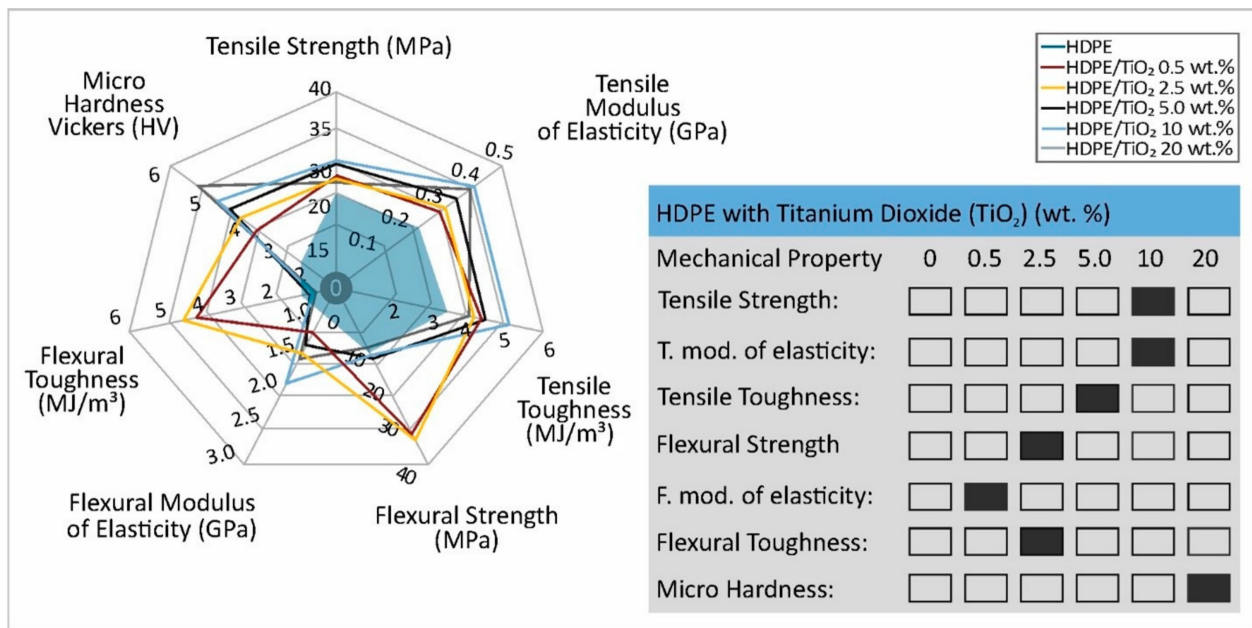


**Figure 11.** Overall mechanical properties results for HDPE with TiO<sub>2</sub> as filler.

The above results are unique in the literature and offer a new aspect of 3D printing that can more effectively implement HDPE material and its micro or nanocomposites as novel and more durable nano/micro composite filaments. The bulk materials of HDPE with TiO<sub>2</sub> can also be used in large-scale production in all types of industries that benefit from extrusion systems. It should be noted also that the increase in the cost for achieving such an enhancement in the mechanical strength of the HDPE polymer is not significant. The increase is mainly due to the additional cost of the additive. HDPE costs about 6 €/kg for laboratory-scale use and this price can be significantly lowered for industrial-scale use. TiO<sub>2</sub> for industrial-scale use costs about 3 €/kg, so for the 10 wt.% nanocomposite, for each kg of HDPE, the increase in the cost of the raw materials to produce the nanocomposite is 0.3€. For the 2.5 wt.% concentration that achieved the highest flexural strength in the study, this cost is 0.075 €/kg of the nanocomposite. The increase in the cost of the process is negligible.

The overall key points from the current research are summarized as follows:

- Mechanically improved HDPE nano/micro composite filament was fabricated using extrusion melting
- There was an increase of 77.6% in flexural strength with the introduction of 2.5 wt.% TiO<sub>2</sub> to the HDPE matrix
- The overall thermal properties were not affected
- The printability of the specimens became difficult after 10% filler loading.

**Author Contributions:** Conceptualization, N.V. and M.P.; methodology, A.M. (Athena Maniadi); software, A.M. (Athena Maniadi) and V.P.; validation, N.V., M.P. and A.M. (Athena Maniadi); formal analysis, A.M. (Athena Maniadi), A.M. (Alexandra Manousaki) and V.P.; investigation, A.M. (Athena Maniadi); resources, N.V.; data curation, A.M. (Athena Maniadi); writing—original draft preparation, A.M. (Athena Maniadi); writing—review and editing, M.P.; visualization, A.M. (Alexandra Manousaki); supervision, N.V.; project administration, N.V.; funding acquisition, M.P. All authors have read and agreed to the published version of the manuscript.

**Funding:** This research received no external funding.

**Institutional Review Board Statement:** Not applicable.

**Informed Consent Statement:** Not applicable.

**Data Availability Statement:** The data presented in this study are available upon request from the corresponding author.

**Acknowledgments:** Authors would like to thank the Institute of Electronic Structure and Laser of the Foundation for Research and Technology-Hellas (IESL-FORTH) and the Photonic Phononic and Meta-Materials Laboratory for sharing the Raman Instrumentation.

**Conflicts of Interest:** The authors declare no conflict of interest.

## References

1. Wu, H.; Fahy, W.P.; Kim, S.; Kim, H.; Zhao, N.; Pilato, L.; Kafi, A.; Bateman, S.; Koo, J.H. Recent developments in polymers/polymer nanocomposites for additive manufacturing. *Prog. Mater. Sci.* **2020**, *111*, 100638. [[CrossRef](#)]
2. Coykendall, J.; Cotteleer, M.; Holdowsky, L.; Mahto, M. *3D Opportunity in Aerospace and Defense*; Deloitte University Press: Westlake, TX, USA, 2014; pp. 1–28.
3. Stansbury, J.W.; Idacavage, M.J. 3D printing with polymers: Challenges among expanding options and opportunities. *Dent. Mater.* **2016**, *32*, 54–64. [[CrossRef](#)] [[PubMed](#)]
4. Tack, P.; Victor, J.; Gemmel, P.; Annemans, L. 3D-printing techniques in a medical setting: A systematic literature review. *Biomed. Eng. Online* **2016**, *15*, 115. [[CrossRef](#)]
5. Vidakis, N.; Petousis, M.; Maniadi, A.; Koudoumas, E.; Vairis, A.; Kechagias, J. Sustainable additive manufacturing: Mechanical response of acrylonitrile-butadiene-styrene over multiple reprocessing processes. *Sustainability* **2020**, *12*, 3568. [[CrossRef](#)]
6. Vidakis, N.; Petousis, M.; Tzounis, L.; Maniadi, A.; Velidakis, E.; Mountakis, N.; Papageorgiou, D.; Liebscher, M.; Mechtcherine, V. Sustainable Additive Manufacturing: Mechanical Response of Polypropylene over Multiple Reprocessing Processes. *Sustainability* **2020**, *13*, 159. [[CrossRef](#)]
7. Vidakis, N.; Petousis, M.; Maniadi, A. Sustainable Additive Manufacturing: Mechanical Response of High-Density Polyethylene over Multiple Reprocessing Processes. *Reprocessing* **2021**, *6*, 4. [[CrossRef](#)]
8. Vidakis, N.; Petousis, M.; Vairis, A.; Savvakis, K.; Maniadi, A. A parametric determination of bending and Charpy's impact strength of ABS and ABS-plus fused deposition modeling specimens. *Prog. Addit. Manuf.* **2019**, *4*, 323–330. [[CrossRef](#)]
9. Sood, A.K.; Ohdar, R.K.; Mahapatra, S.S. Experimental investigation and empirical modelling of FDM process for compressive strength improvement. *J. Adv. Res.* **2012**, *3*, 81–90. [[CrossRef](#)]
10. Galantucci, L.M.; Lavecchia, F.; Percoco, G. Study of compression properties of topologically optimized FDM made structured parts. *CIRP Ann.-Manuf. Technol.* **2008**, *57*, 243–246. [[CrossRef](#)]
11. Vairis, A.; Petousis, M.; Vidakis, N.; Savvakis, K. On the Strain Rate Sensitivity of Abs and Abs Plus Fused Deposition Modeling Parts. *J. Mater. Eng. Perform.* **2016**, *25*, 3558–3565. [[CrossRef](#)]
12. Vidakis, N.; Petousis, M.; Korlos, A.; Velidakis, E.; Mountakis, N.; Charou, C.; Myftari, A. Strain Rate Sensitivity of Polycarbonate and Thermoplastic Polyurethane for Various 3D Printing Temperatures and Layer Heights. *Polymers* **2021**, *13*, 2752. [[CrossRef](#)] [[PubMed](#)]
13. Vidakis, N.; Petousis, M.; Kechagias, J.D. A comprehensive investigation of the 3D printing parameters' effects on the mechanical response of polycarbonate in fused filament fabrication. *Prog. Addit. Manuf.* **2022**, 1–10. [[CrossRef](#)]
14. Vidakis, N.; Petousis, M.; Maniadi, A.; Koudoumas, E.; Liebscher, M.; Tzounis, L. Mechanical properties of 3D-printed acrylonitrile-butadiene-styrene TiO<sub>2</sub> and ATO nanocomposites. *Polymers* **2020**, *12*, 1589. [[CrossRef](#)] [[PubMed](#)]
15. Vidakis, N.; Petousis, M.; Maniadi, A.; Koudoumas, E.; Kenanakis, G.; Romanitan, C.; Tutunaru, O.; Sucheai, M.; Kechagias, J. The mechanical and physical properties of 3D-Printed materials composed of ABS-ZnO nanocomposites and ABS-ZnO micro composites. *Micromachines* **2020**, *11*, 615. [[CrossRef](#)] [[PubMed](#)]
16. Vidakis, N.; Maniadi, A.; Petousis, M.; Vamvakaki, M.; Kenanakis, G.; Koudoumas, E. Mechanical and Electrical Properties Investigation of 3D-Printed Acrylonitrile–Butadiene–Styrene Graphene and Carbon Nanocomposites. *J. Mater. Eng. Perform.* **2020**, *29*, 1909–1918. [[CrossRef](#)]
17. Vidakis, N.; Petousis, M.; Velidakis, E.; Mountakis, N.; Tzounis, L.; Liebscher, M.; Grammatikos, S.A. Enhanced mechanical, thermal and antimicrobial properties of additively manufactured polylactic acid with optimized nano silica content. *Nanomaterials* **2021**, *11*, 1012. [[CrossRef](#)] [[PubMed](#)]
18. Vidakis, N.; Petousis, M.; Savvakis, K.; Maniadi, A.; Koudoumas, E. A comprehensive investigation of the mechanical behavior and the dielectrics of pure polylactic acid (PLA) and PLA with graphene (GnP) in fused deposition modeling (FDM). *Int. J. Plast. Technol.* **2019**, *23*, 195–206. [[CrossRef](#)]
19. Alzerreca, M.; Paris, M.; Boyron, O.; Orditz, D.; Louarn, G.; Correc, O. Mechanical properties and molecular structures of virgin and recycled HDPE polymers used in gravity sewer systems. *Polym. Test.* **2015**, *46*, 1–8. [[CrossRef](#)]
20. Coulier, L.; Orbons, H.G.M.; Rijk, R. Analytical protocol to study the food safety of (multiple-)reprocessed high-density polyethylene (HDPE) and polypropylene (PP) crates: Influence of reprocessing on the migration and formation of degradation products. *Polym. Degrad. Stab.* **2007**, *92*, 2016–2025. [[CrossRef](#)]
21. Simões, C.L.; Costa Pinto, L.M.; Bernardo, C.A. Environmental and economic assessment of a road safety product made with pure and reprocessed HDPE: A comparative study. *J. Environ. Manag.* **2013**, *114*, 209–215. [[CrossRef](#)]
22. Achilias, D.S.; Roupakias, C.; Megalokonomos, P.; Lappas, A.A.; Antonakou, V. Chemical reprocessing of plastic wastes made from polyethylene (LDPE and HDPE) and polypropylene (PP). *J. Hazard. Mater.* **2007**, *149*, 536–542. [[CrossRef](#)] [[PubMed](#)]

23. Vries, C.D. *Volkswagen Autoeuropa: Maximizing Production Efficiency with 3D Printed Tools, Jigs, and Fixtures*; Ultimaker: Utrecht, The Netherlands, 2017; Volume 26.
24. Xiao, K.Q.; Zhang, L.C.; Zarudi, I. Mechanical and rheological properties of carbon nanotube-reinforced polyethylene composites. *Compos. Sci. Technol.* **2007**, *67*, 177–182. [[CrossRef](#)]
25. Bharath, K.; Doddamani, M.; Zeltmann, S.E.; Gupta, N.; Ramesh, M.R.; Ramakrishna, S. Processing of cenosphere/HDPE syntactic foams using an industrial scale polymer injection molding machine. *Mater. Des.* **2016**, *92*, 414–423. [[CrossRef](#)]
26. Bharath, K.; Doddamani, M.; Zeltmann, S.E.; Gupta, N.; Gurupadu, S.; Sailaja, R.R.N. Effect of particle surface treatment and blending method on flexural properties of injection-molded cenosphere/HDPE syntactic foams. *J. Mater. Sci.* **2016**, *51*, 3793–3805. [[CrossRef](#)]
27. Bharath, K.; Doddamani, M.; Zeltmann, S.E.; Gupta, N.; Gurupadu, S.; Sailaja, R.R.N. Effect of cenosphere surface treatment and blending method on the tensile properties of thermoplastic matrix syntactic foams. *J. Appl. Polym. Sci.* **2016**, 43881. [[CrossRef](#)]
28. Jayavardhan, M.L.; Bharath, K.; Doddamani, M.; Singh, A.K.; Zeltmann, S.E.; Gupta, N. Development of glass microballoon/HDPE syntactic foams by compression molding. *Compos. B Eng.* **2017**, *130*, 119–131. [[CrossRef](#)]
29. Jayavardhan, M.L.; Doddamani, M. Quasi-static compressive response of compression molded glass microballoon/HDPE syntactic foam. *Compos. B Eng.* **2018**, *149*, 165–177. [[CrossRef](#)]
30. Doddamani, M. Influence of microballoon wall thickness on dynamic mechanical analysis of closed cell foams. *Mater. Res. Express* **2020**, *6*, 125348. [[CrossRef](#)]
31. Fouad, H.; Elleithy, R.; Al-Zahrani, S.M.; Ali, M.A.-H. Characterization and processing of high density polyethylene/carbon nano-composites. *Mater. Des.* **2011**, *32*, 1974–1980. [[CrossRef](#)]
32. Yuan, Q.; Yang, Y.; Chen, J.; Ramuni, V.; Misra, R.D.K.; Bertrand, K.J. The effect of crystallization pressure on macromolecular structure, phase evolution, and fracture resistance of nano-calcium carbonate-reinforced high density polyethylene. *Mater. Sci. Eng. A* **2010**, *527*, 6699–6713. [[CrossRef](#)]
33. Di, W.; Zhang, G.; Xu, J.; Peng, Y.; Wang, X.; Xie, Z. Positive-temperature-coefficient/negative-temperature-coefficient effect of low-density polyethylene filled with a mixture of carbon black and carbon fiber. *J. Polym. Sci. B Polym. Phys.* **2003**, *41*, 3094–3101. [[CrossRef](#)]
34. Azeez, A.; Rhee, K.Y.; Park, S.-J.; Hui, D. Epoxy clay nanocomposites—Processing, properties and applications: A review. *Compos. B Eng.* **2013**, *45*, 308–320. [[CrossRef](#)]
35. Beesetty, P.; Kale, A.; Patil, B.; Doddamani, M. Mechanical behavior of additively manufactured nanoclay/HDPE nanocomposites. *Compos. Struct.* **2020**, *247*, 112442. [[CrossRef](#)]
36. Akhil, P.S.; Golla, B.R.; James, A.R. Characterization of high  $\kappa$  HDPE-TiO<sub>2</sub> composites: A first report. *Mater. Lett.* **2019**, *241*, 128–131. [[CrossRef](#)]
37. Shirkavand, M.J.; Azizi, H.; Ghasemi, I.; Karabi, M. Effect of Molecular Structure Parameters on Crystallinity and Environmental Stress Cracking Resistance of High-Density Polyethylene/TiO<sub>2</sub> Nanocomposites. *Adv. Polym. Technol.* **2018**, *37*, 770–777. [[CrossRef](#)]
38. Anu, M.A.; Pillai, S.S. Structure, thermal, optical and dielectric properties of SnO<sub>2</sub> nanoparticles-filled HDPE polymer. *Solid State Commun.* **2022**, *341*, 114577. [[CrossRef](#)]
39. Wang, H.; Yang, D.; Xiong, W.; Liu, W.; Qiu, X. One-pot preparation of hydrophobic lignin/SiO<sub>2</sub> nanoparticles and its reinforcing effect on HDPE. *Int. J. Biol. Macromol.* **2021**, *180*, 523–532. [[CrossRef](#)]
40. Mahmoud, M.E.; El-Khatib, A.M.; Badawi, M.S.; Rashad, A.R.; El-Sharkawy, R.M.; Thabet, A.A. Fabrication, characterization and gamma rays shielding properties of nano and micro lead oxide-dispersed-high density polyethylene composites. *Radiat. Phys. Chem.* **2018**, *145*, 160–173. [[CrossRef](#)]
41. Mahmoud, M.E.; Khalifa, M.A.; El-Sharkawy, R.M.; Youssef, M.R. Effects of Al<sub>2</sub>O<sub>3</sub> and BaO nano-additives on mechanical characteristics of high-density polyethylene. *Mater. Chem. Phys.* **2021**, *262*, 124251. [[CrossRef](#)]
42. Benabid, F.Z.; Kharchi, N.; Zouai, F.; Mourad, A.H.I.; Benachour, D. Impact of co-mixing technique and surface modification of ZnO nanoparticles using stearic acid on their dispersion into HDPE to produce HDPE/ZnO nanocomposites. *Polym. Polym. Compos.* **2019**, *27*, 389–399. [[CrossRef](#)]
43. Bedi, P.; Singh, R.; Ahuja, I.P.S. Investigations for tool life of 3D printed HDPE and LDPE composite based rapid tooling for thermoplastics machining applications. *Eng. Res. Express* **2019**, *1*, 015003. [[CrossRef](#)]
44. Oblak, P.; Gonzalez-Gutierrez, J.; Zupančič, B.; Aulova, A.; Emri, I. Processability and mechanical properties of extensively recycled high density polyethylene. *Polym. Degrad. Stab.* **2015**, *114*, 133–145. [[CrossRef](#)]
45. Bednarik, M.; Manas, D.; Ovsik, M.; Manas, M.; Stanek, M.; Sanda, S.; Kratky, P. Effect of beta irradiation on the strength of bonded joints of HDPE. *Key Eng. Mater.* **2014**, *586*, 79–82. [[CrossRef](#)]
46. Crosby, A.J.; Lee, J.Y. Polymer nanocomposites: The “nano” effect on mechanical properties. *Polym. Rev.* **2007**, *47*, 217–229. [[CrossRef](#)]
47. Perevedentseva, E.; Lin, Y.C.; Karmenyan, A.; Wu, K.T.; Lugovtsov, A.; Shirshin, E.; Priezzhev, A.; Cheng, C.L. Raman Spectroscopic Study of TiO<sub>2</sub> Nanoparticles’ Effects on the Hemoglobin State in Individual Red Blood Cells. *Materials* **2021**, *14*, 5920. [[CrossRef](#)]
48. Stuart, B.H. Temperature studies of polycarbonate using Fourier transform Raman spectroscopy. *Polym. Bull.* **1996**, *36*, 341–346. [[CrossRef](#)]

49. Resta, V.; Quarta, G.; Lomascolo, M.; Maruccio, L.; Calcagnile, L. Raman and Photoluminescence spectroscopy of polycarbonate matrices irradiated with different energy Si-28(+) ions. *Vacuum* **2015**, *116*, 82–89. [[CrossRef](#)]
50. Zimmerer, C.; Matulaitiene, G.; Niaura, G.; Reuter, U.; Janke, A.; Boldt, R.; Sablinskas, V.; Steiner, G. Nondestructive characterization of the polycarbonate-octadecylamine interface by surface enhanced Raman spectroscopy. *Polym. Test.* **2019**, *73*, 152–158. [[CrossRef](#)]
51. Makarem, M.; Lee, C.M.; Kafle, K.; Huang, S.X.; Chae, I.; Yang, H.; Kubicki, J.D.; Kim, S.H. Probing cellulose structures with vibrational spectroscopy. *Cellulose* **2019**, *26*, 35–79. [[CrossRef](#)]
52. Liu, X.B.; Zou, Y.B.; Li, W.T.; Cao, G.P.; Chen, W.J. Kinetics of thermo-oxidative and thermal degradation of poly(D,L-lactide) (PDLLA) at processing temperature. *Polym. Degrad. Stab.* **2006**, *91*, 3259–3265. [[CrossRef](#)]